

# Digital processing of multi-mode nano-mechanical cantilever data

T Braun<sup>1</sup>, M K Ghatkesar<sup>1</sup>, V Barwich, N Backmann, F Huber, W Grange, N Nugaeva, H P Lang, J P Ramseyer, Ch Gerber and M Hegner

National Center of Competence for Research in Nanoscience, Institute of Physics, University of Basel, 4056 Basel, Switzerland

**Abstract.** Nanomechanical sensors based on cantilever technology allow the measurement of various physical properties. Here we present a software for the comprehensive analysis of such data. An example for the combined measurement of mass and surface stress is presented.

## 1. Introduction

Ideally a biosensor for membrane protein receptors should be able to detect three physical changes upon ligand binding: (i) the mass-increase caused by the ligand, (ii) the conformational change of the receptor by which it transmits the signal and (iii) the change of the membrane potential. All the above criteria can be fulfilled by micromechanical cantilever based sensors: (i) In the dynamic mode the mass increase on the cantilever due to ligand adsorption is measured by tracking the eigenfrequency at higher harmonics. (ii) In the static mode, conformational changes of receptors, charge effects and/or sterical competition between different ligand molecules on the sensor surface lead to a bending of the cantilever. (iii) To measure the membrane potential, the voltage between the conducting cantilever surface and the surrounding buffer can be measured. Theoretically, all detection modes can be recorded in parallel facilitating a comprehensive interpretation of the data. We propose that the physical signals measured are directly correlated to biologically relevant properties. This applies for the absolute absorbed mass [1] and for the structural changes of membrane proteins [2]. Of course, these two physical changes should also be measurable for soluble receptor molecules.

This unique combination of different physically measured properties in parallel needs new software for efficient data analysis. Furthermore, some techniques do not record directly the desired parameters versus time and have to be first post-processed after the experiment before a conclusive discussion can be performed (see figure 1). In the case of dynamic mode data the frequency is not tracked directly by a phase lock loop system (PLL) but by recording response spectra (amplitude, phase) in dependence of the excitation frequency. From the raw data, various properties can be extracted such as damping and the absolute mass of the ligand bound to the cantilever. Here we describe a new software, called NOSEtools, for the semi-automated handling, processing and presentation of such sensor data.

<sup>1</sup> Equally contributed

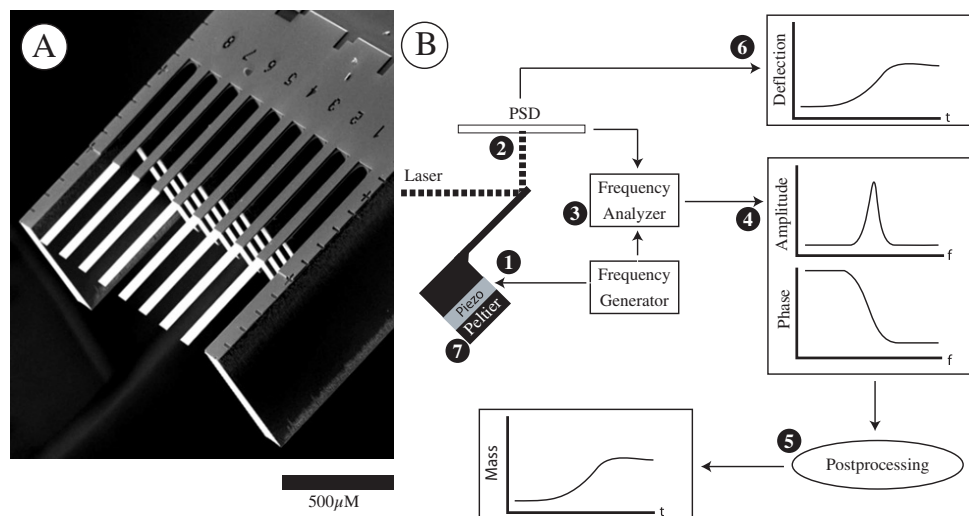


**Figure 1.** Instrument set-up. A) Cantilever array with 8 cantilevers between two protection outer bars. B) A frequency generator sweeps the spectrum by exciting a piezoelectric actuator located beneath the base of the microcantilever array chip (1). The response of the cantilever is optically detected with a laser using a position-sensitive detector (PSD, 2). The frequency analyzer (3) compares the cantilever response with the excitation from the frequency generator to determine the phase. Amplitude and phase spectra are continuously recorded (4). To get the adsorbed mass, a post-processing is needed (5). In contrast to that, the static mode data is directly recorded as deflection versus time (6). The temperature is controlled by a peltier element (7).

## 2. Data organization

The mix of time-scaled measurements (*e.g.* cantilever deflection versus time) and non-time scaled measurements needs special organization of the data structure in the software: Raw data are stored in so called projects and all calculations are performed in instances. All data in instances are time-scaled and can be compared directly. Dynamic mode data of recorded spectra per time point has to be post-processed and the results are stored in the instance. A flow-diagram of this separation is depicted in figure 2 in comparison to the graphical implementation of the software.

## 3. Post processing

Recorded time series of spectra can be analyzed using two methods: 1.) Amplitude peak-tracking and phase-turning point tracking [3]. 2.) Least-mean square fitting of the spectrum. This method involved the fitting of the amplitude and of the corresponding phase spectrum by the model described in Section 3.2.

### 3.1. Amplitude-peak and phase tracking

Here a phenomenological interpretation of the data is performed without underlying model or assumptions. The algorithms extract geometrical properties of the recorded spectra, such as peak-maximum frequency, peak-height (amplitude), Q-factor for the amplitude spectra, and the turn-point of the phase. Figure 3 depicts the rough algorithm used for these data extractions.

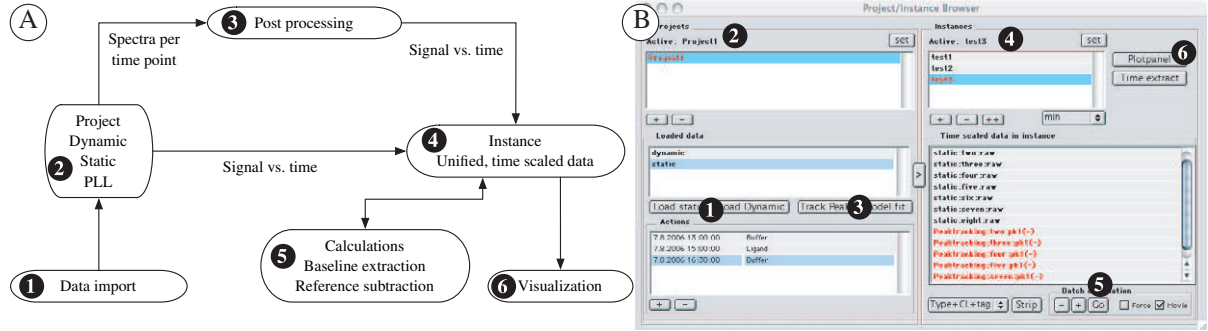


**Figure 2.** Organization of the data handling in the NOSEtool software. A) Diagram of the data flow in the software. B) User interface for the data control representing the diagram of A. (1) Data import for raw data. (2) Projects: contains raw data and all associated informations. (3) Post processing tools for non-time-scaled data. (4) Instances: contains time scaled data. Here all calculations (baseline correction, reference subtraction) take place (5), (6) Visualization of the time-scaled data in graphs.

### 3.2. Modeling of data

The model used in this part of the software is described in detail elsewhere [1]. The eigenfrequencies for mode  $n$  of a rectangular cantilever that has a distributed mass in the absence of damping are described in analogy to the model of a harmonic oscillator by

$$f_{0n} = \frac{\alpha_n^2}{2\pi} \sqrt{\frac{k}{3(m_{tot})}}. \quad (1)$$

with  $k$  as the spring constant and  $m_{tot}$  the total mass of the cantilever. (The  $\alpha_n$  are related to the different eigenvalues of the harmonics and are fixed by the boundary conditions [4].) The fit function of the resonance peak of an amplitude spectrum was based on the amplitude response function  $u(f)$  of Eq. (2) and the model for the phase response is based on Eq. (3).

$$u_n(f) = \frac{u_{\max} f_{0n}^2}{\sqrt{(f_{0n}^2 - f^2)^2 + \frac{\gamma^2 f^2}{\pi^2}}} \quad (2) \quad \varphi(f) = \arctan \frac{-\gamma f}{\pi(f_{0n}^2 - f^2)} \quad (3)$$

( $u_{\max}$ : driving amplitude,  $f_{0n}$ : eigenfrequency of Eq. 1 for mode  $n$ ,  $\gamma$ : damping.)

For spectra exhibiting several peaks, a superposition of peaks or phase transitions was fitted to the complete spectra.  $m_{tot}$  of Eq. (1) includes the mass of the cantilever itself ( $m_c$ ), the absorbed mass ( $m_{abs}$ ) and the virtual mass of the liquid ( $m_l$ ) which is moved with the cantilever vibration. The latter virtual mass  $m_l$  is unknown, depends on the system and has to be calibrated at the beginning of the measurement to be able to measure the absolute bound mass after ligand injection. A flow diagram of the involved steps in the post-processing is depicted in figure 3. Note that this evaluation method measures the absolute mass directly after calibration. From this also the resonance amplitude peak-frequencies and eigenfrequencies can be calculated.

## 4. Example

To test the combined mode of sensing dynamic and static information at the same time, a standard temperature test was performed. To do this test, the cantilever array shown in figure 1 was covered with 20 nm gold on one side of the cantilevers, mounted in the measurement

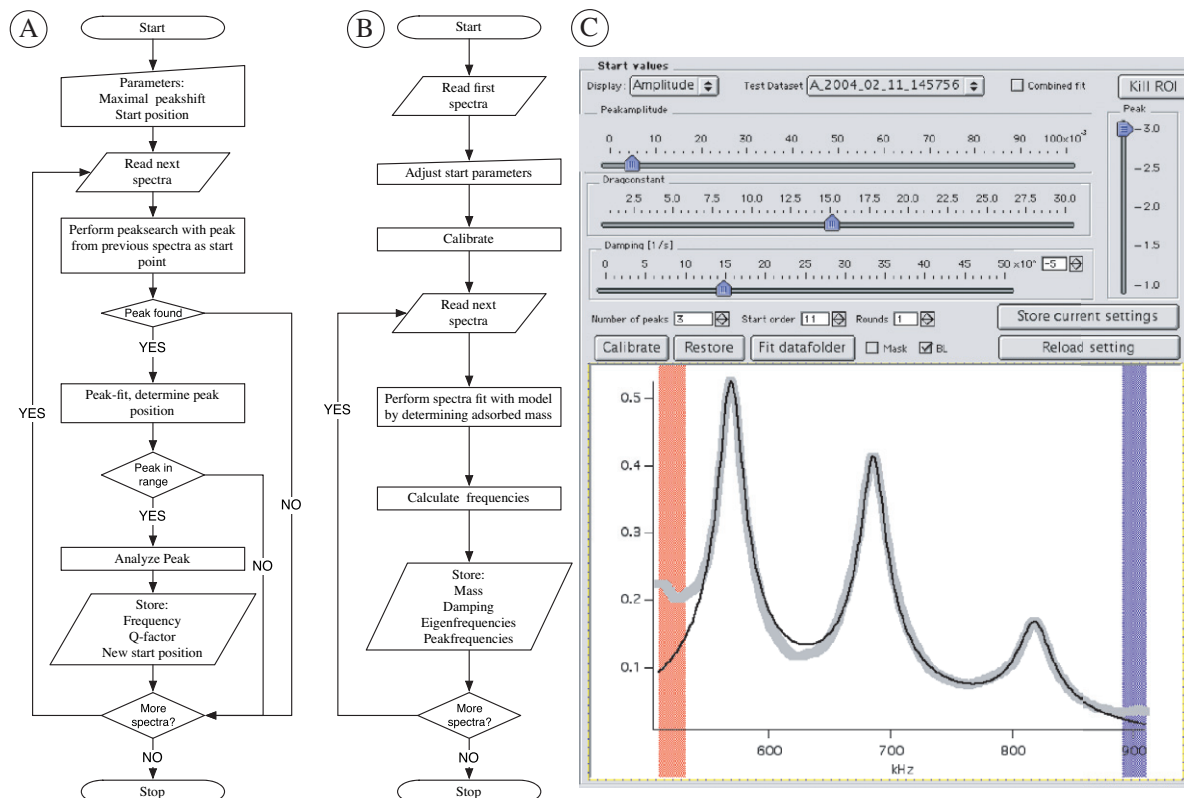


**Figure 3.** Simplified flow diagram for peak tracking and model fit algorithms. A) The peak-tracking procedure reads in one spectrum after the other. The user provides start position and a maximal peak-shift for the peak-search which propagates from spectrum to spectrum. Note that a Gauss fit or Lorenz fit is used to minimize the effect of noise instead of data smoothing. For the phase data a analogue algorithm was used. B) work flow for mass determination by modeling a series of spectra. C) Graphical user interface for model fitting. Note the preview-window with the raw data (thick grey line) and the model fit in black.

chamber and immersed in buffer. After ensuring stable baselines for both static and dynamic mode data, the chamber was exposed to a temperature pulse of about 5 K in a period of 3 min.

The results of the heat test are depicted in figure 4. Panel A shows the static bending of all cantilever arrays, panel B the change of the virtual mass of the co-moving liquid after post-processing with the model described in section 3.2 (amplitude spectra).

In the static mode, a clear bending of the cantilever is observed during the heating period. The mechanical energy for this work originates from the different thermal expansion-coefficients of gold ( $14.2 \times 10^{-6} \text{ K}^{-1}$ ) and silicon ( $2.6 \times 10^{-6} \text{ K}^{-1}$ ) leading to a “bimetal” effect. The cantilever bends towards the silicon interface as thermal expansion coefficient of gold is larger than silicon. The uniformity of the cantilever response demonstrates the high mechanical quality of the cantilevers.

In the dynamic signal, the virtual mass of the co-moving liquid, is lowered by the heat pulse. This observation is in agreement with the expectations that the density of the buffer is lower and intermolecular interactions are weaker between liquid molecules at higher temperature. However, the response shows a large variation in the mass among different cantilevers. The measured mass changes increased depending on the position of the cantilever in the array: The further away from

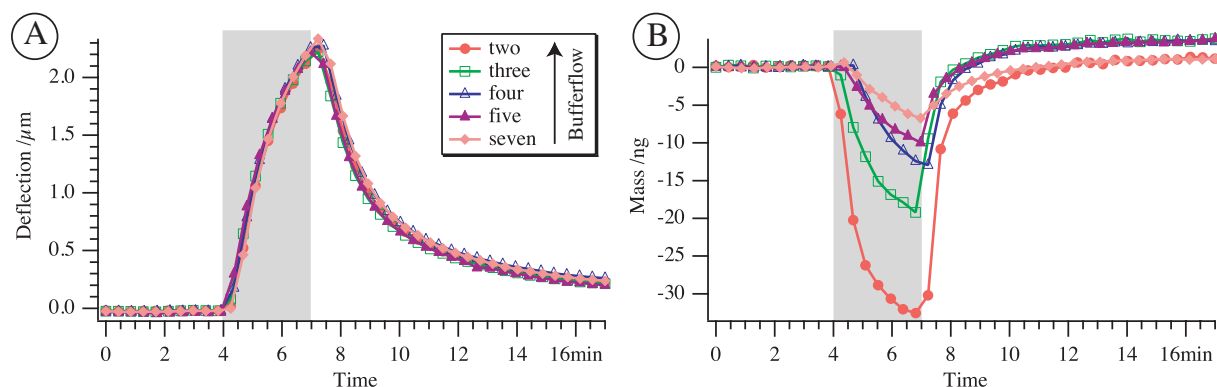


**Figure 4.** Heat test of a cantilever array immersed in buffer. The heating period is indicated in gray. A) static deflection signal, B) Dynamic signal after post-processing by modeling the amplitude spectra. The flow of buffer is indicated in the inset.

the buffer inlet the larger the mass change (see inset in figure 4). The explanation is found in the temperature control of the system: The heat pulse is performed by a thermoelement beneath the cantilever array (figure 1). This ensures a good thermal coupling with the cantilever array which is heated homogeneously for all cantilevers. In contrast to that, the buffer has to be heated up first by the chamber and due to the constant buffer-flow ( $12 \mu\text{l}/\text{min}$ ) a temperature gradient builds in the liquid of the measurement cell (volume:  $5 \mu\text{l}$ ). Therefore different cantilevers experience different local liquid characteristics.

The signals of static and dynamic modes measured in parallel are in good agreement and reflect the characteristics they are sensing in response to the heat test: The static mode assesses the internal reaction of the cantilever on heat, whereas the dynamic mode senses changes in the environment.

## 5. Conclusions

Here we present a software tool developed for the efficient analysis of multimode cantilever data. The presented example demonstrates the potential of combined measurements for static and dynamic mode, sensing different characteristics of the system.

## Material and Methods

All data-processing algorithms were implemented in the IGOR PRO (Wavemetrics, Portland, USA) data analyze environment. The complete NOSEtools software package is currently in private beta testing and can be obtained upon request when the final release is ready. Piranha-cleaned cantilever arrays (IBM Zurich Research Laboratory, Switzerland;  $500 \mu\text{m}$  long,  $100 \mu\text{m}$  wide,  $1 \mu\text{m}$  thick,  $0.03 \text{ N/m}$ ) were coated with  $3 \text{ nm}$  Ti adhesion layer followed by  $20 \text{ nm}$  Au by evaporation (Balzers MED 010). The complete experiment was performed in a continuous buffer ( $10 \text{ mM}$  HEPES pH 7.4,  $150 \text{ mM}$  NaCl) flow of  $12 \mu\text{l}/\text{min}$ . Cantilever 1, 6 and 8 were ignored due to bad alignment with the laser beam.

## References

- [1] Braun T, Barwich V, Ghatkesar M K, Bredekamp A H, Gerber Ch, Hegner M, and Lang H P. *Physical Review E.*, (72):031907, 2005.
- [2] Braun T, Backmann N, Bietsch A, Gerber Ch, Lang H P, and Hegner M. *Biophys. J.*, 90(8):2970–2977, 2006.
- [3] Ghatkesar M K, Barwich V, Braun T, Bredekamp A B, Drechsler U, Despont M, Lang H P, Hegner M, and Gerber Ch. *IEEE Sensors*, pages 1060–1063, 2004.
- [4] Young D and Robert P. Felgar, jr. *The University of Texas Publication*, 44(4913):1–32, 1949.